

Non-Linear Dynamics of Cylindrical Tubes in a Cross-Flow Heat-Exchanger

Vinu V

A Thesis Submitted to
Indian Institute of Technology Hyderabad
In Partial Fulfillment of the Requirements for
The Degree of Master of Technology



भारतीय प्रौद्योगिकी संस्थान हैदराबाद
Indian Institute of Technology Hyderabad

Department of Mechanical and Aerospace Engineering

June 2015

Declaration

I declare that this written submission represents my ideas in my own words, and where ideas or words of others have been included, I have adequately cited and referenced the original sources. I also declare that I have adhered to all principles of academic honesty and integrity and have not misrepresented or fabricated or falsified any idea/data/fact/source in my submission. I understand that any violation of the above will be a cause for disciplinary action by the Institute and can also evoke penal action from the sources that have thus not been properly cited, or from whom proper permission has not been taken when needed.



(Signature)

(Vinu V)

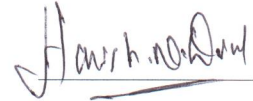
(Roll No. ME13M1016)

Approval Sheet

This Thesis entitled Non-Linear Dynamics of Cylindrical Tubes in a Cross-Flow Heat-Exchanger by Vinu V is approved for the degree of Master of Technology from IIT Hyderabad



(Dr. N. R. Aravind) Examiner
Dept of Computer Science and Engineering, IITH



(Dr. Harish N Dixit) Examiner
Dept. of Mechanical and Aerospace Engineering, IITH



(Dr. Chandrika Prakash Vyasarayani) Adviser
Dept. of Mechanical and Aerospace Engineering, IITH



(Dr. Viswanath Chinthapenta) Chairman
Dept. of Mechanical and Aerospace Engineering, IITH

Acknowledgements

I would like to express my gratitude to all those who helped me to finish my thesis. First and foremost I would like to thank God, the almighty, for giving me strength and courage to do research.

I would like to thank my parents and siblings for their love, endless support and encouragement.

I express my sincere gratitude to my supervisor Dr. V. C. Prakash for his inspiration, valuable guidance, timely suggestions and constant encouragement during each and every phase of this work.

Finally, I would like to thank all my friends Anwar, Zaid, Samukham, Harilal, Ajmal, and Kumar for supporting me to finish my work.

Dedication

*This thesis is dedicated to my parents & siblings
for their love, endless support
and encouragement*

Abstract

In this thesis, a mathematical model of a single flexible cylinder in an array of rigid cylinders subjected to cross-flow is studied. The flexible tube is subjected to an initial axial load and supported by loose supports. The instability and nonlinear dynamics of tubes planar motions are taken into consideration. Numerical results are obtained using a five-mode discretization of the governing equation. The results obtained thus indicate that, with high axial loads and flow velocities beyond certain critical values, the system can undergo flutter or buckling instability. The instability regions and its boundaries are predicted analytically. These boundaries indicate that for a particular initial axial load, with increasing flow velocity beyond a critical value, amplitude of vibration grows until it impacts with the loose support, thereby more complex motion arise leading to chaos.

Contents

| | |
|---|------------|
| Declaration | ii |
| Approval Sheet | iii |
| Acknowledgements | iv |
| Abstract | vi |
| Nomenclature | vii |
| 1 Introduction | 1 |
| 1.1 Literature review | 2 |
| 1.2 Problem definition | 4 |
| 1.3 Thesis structure | 4 |
| 2 The flow-induced forces on a flexible tube | 5 |
| 2.1 Fluid forces and flow retardation | 5 |
| 3 Mathematical modelling | 8 |
| 4 Stability and bifurcation analysis | 12 |
| 4.1 Stability Analysis | 12 |
| 4.2 Bifurcation Analysis | 14 |
| 4.2.1 Cubic Spring model | 14 |
| 4.2.2 Trilinear Spring model | 17 |
| 5 Conclusions | 26 |
| References | 27 |

Chapter 1

Introduction

Fluid induced vibration of tubular cylinders is a major concern while designing the powerplant heat-exchangers. Any failure caused in this particular component may leads to outrageous disaster. Fluid structure interaction (FSI) is one of the main reason for generating vibrations in elastic structures. Earlier FSI was considered as a secondary design criteria, but the advent of high strength materials leading to the manufacturing of slender tubes and the high fluid-flow velocity applications in nuclear power plants, the effect of FSI became substantial [1].

The vibration due to FSI are mainly because of vortex shedding, turbulent buffeting and fluid-elastic instability (FEI). Vortex shedding occurs when the frequency of periodic excitation coincides with the mechanical resonant frequency of the tubes. Turbulent buffeting is the excitation caused due to change in velocity at the periphery of the tubes [2]. FEI is basically a feedback mechanism between the structural motion and the resulting fluid forces. In FEI, a small displacement of the heat exchanger tube alters the flow pattern and leads to a change in fluid force, this in turn leads to a further displacement change and so on. Hence, it is a positive feedback mechanism [3] and which to FEI. Excitations caused due to vortex shedding and turbulent buffeting can be neglected because it is controlled by the inherent damping. However, the vibrations due to the FEI can cause severe damage to the structure in a very small time span. In this thesis we are interested to study the effects of FEI in heat-exchanger tubes subjected to cross-flow.

Mainly two mechanisms are generally responsible for fluid-elastic instability. The first one is a velocity controlled negative damping mechanism and the second one is a stiffness controlled mechanism. It is well known that, the velocity controlled negative damping mechanism is responsible for fluid-elastic instability in a rotated triangular and square arrays of tube configurations, if the mass damping parameter agrees the relation $^1m\delta/\rho D^2 < 300$ [4]. At critical fluid flow velocity, due to the interplay between the structural motion and the fluid flow, the net damping in the structure becomes zero, leading to the FEI. Typically gaps are provided at the tube supports to account thermal expansion of tubes. So at higher flow velocity beyond the critical flow velocity, the response of the system grows suddenly and that leads to violent impacts between the pipe and the supports. If the amplitude of post FEI oscillations are huge, the pipes can impact the neighboring tubes. This vibro-impacting motions of the tubes will leads to ratcheting and fatigue stress on the tubes at impact locations.

¹ m is the cylinder mass per unit length, δ is the logarithmic decrement of damping, ρ is the fluid density and D is the cylinder diameter

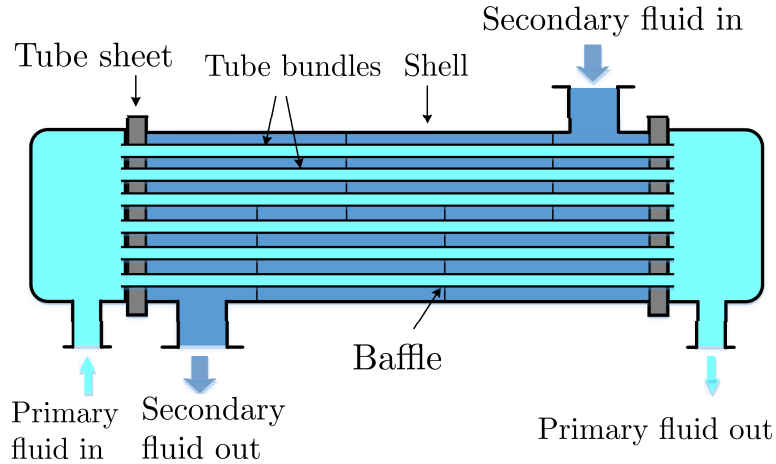


Figure 1.1: A shell and tube Heat exchanger

The fluidelastic instability models have been classified into seven groups as: Jet switch model [5], the quasi-static model [6, 7], the inviscid flow model [8], the quasi-steady model [3], the unsteady model [9], the computational fluid dynamic model [10], and the semi-analytical model [11]. In a shell and tube heat exchanger 1.1, the tubular cylinders are threaded through baffle plates in order to direct the fluid flow and offer support to the tubes. For ease of threading and to allow thermal expansion, a gap is provided between the tube and the baffle plate. Due to overuse, crud may deposit in the gap offering loose-positive support for the tubes. The impact of the heat exchanger tubes with the loose support give rise to structural non-linearities [4]

For the system with loose support, the effect of non-linearity due to mean axial tension is not so pronounced. But in the case of the cylindrical array without loose support, the effect of non-linearity due to mean axial tension has an important role in the prediction of flutter amplitude of the cylindrical tubes. In a recent work by Xia and Wang [12], the effect of non-linearity associated with the mean axial extension of the cylindrical tubes were taken into consideration. The array of cylindrical tubes are subjected to an initial axial load under cross-flow. This initial axial load in the system is either due to externally imposed force or due to thermal expansion of the tubes.

The onset of fluidelastic instability leads to relatively large vibration of the heat exchanger tubes which increases with increasing velocity. Hence, a non-linear analysis of the system is required. Besides, in this study, the non-linearity due to loose supports and the non-linearity due to mean axial tension is also taken into consideration.

1.1 Literature review

The major assumption that has been conceived by many researchers while analysing the FEI of heat exchanger tube was, one flexible tube is surrounded by number of rigid tubes and the entire analysis was focused on dynamics of the flexible tube. Some of the famous works on this topic includes, the works of Paidoussis and Li [4], Wang et al. [13], Xia and Wang [12], and S.J Price and Paioussis [3]. In the literature by Paidoussis and Li [4], the geometry of the cylindrical array was taken in such a way that the negative damping instability is dominant, i.e, mass damping parameter was taken to be less than 300. The heat exchanger pipes were considered as a two-span beam clamped at both

ends with loose support in the middle. A similar approach was used by Wang et al. [14], in which the FEI analysis of cantilever beam with loose support at free end was studied. Xia and Wang [12] studied a system in which the nonlinearity associated with induced tension due to axial deformation was also taken into consideration. In a recent work by Wang et al. [13], the effects of initial axial load in the vibration of cylindrical tubes subjected to cross-flow was investigated.

Several experimental works were conducted for studying the various mechanisms involved in the fluidelastic instability of the tube bundles. A review article by Khalifa et. al. [15] deals with the effect of tube location in a tube-array on FEI of heatexchanger tube. The experiments were carried out with a single flexible tube positioned at various locations in the tube-array, it was found that the tube when placed in the third row of the rigid parallel triangular array became fluidelastically unstable, but no instability behavior was found when it was positioned in the first, second, fourth, or fifth row of the array. It was concluded that the fluidelastic instability is caused due to the combined effect of damping and stiffness mechanisms.

S. J. Price and Paidoussis [16] conducted an experimental study in a wind tunnel on a double row flexible cylinders under overflow to determine the fluid force coefficient data. An investigation on the effects of number of parameters on critical velocity was done. Theoretical and experimental results were compared and was observed to be in agreement with each other.

The review paper of Weaver et. al. [17] provides an overview of the current understanding in the area of flow induced vibration in power and process plant components. Various types of excitation mechanisms namely, turbulence, vorticity shedding, fluidelastic instability, axial flow, and two phase flows were analyzed.

In a recent work by Azizian and Mureithi [18], experimental analysis of the flow-induced vibration in steam generator components was investigated. An empirical model was developed by analyzing the force-displacement relationship and estimation of the parameters involved during tube-support interaction including fluid forces, number and type of supports, and geometry of contact. The empirical model is used to simulate tube support interaction for various gap sizes and excitation forces, the non-linear spring damping model reduces the impact error to less than 20 percent when compared with the experimental test results.

Researchers have proposed several type of mathematical models for analyzing the fluidelastic instability. Roberts [5] proposed jet-switching mechanism in which a semi empirical relation was used to determine the critical velocity (U_c) at which instability occurs.

$$\frac{U_c}{fd} = K \left(\frac{\delta m}{\rho d^2} \right)^{1/2} \quad (1.1)$$

Quasi-static model proposed by connors [6] suggested that the displacement and position of the main tube and the neighboring tubes define the flow pattern and fluid forces on the tubes. A semi-empirical relation similar to roberts [5] was also proposed by Connors, in which critical velocity was calculated as the function of mass-damping parameter. The lift and drag force coefficients were measured as a function of inter-cylinder postions. Quasi-steady model proposed by price and paidoussis [16] assumes that negative damping is the primary effect of instability. The lift and drag forces acting on tube arrays were predicted and found to agree well with experimental data. Unsteady flow model (UFM) takes tubes own motion and motion of neighboring tube to determine the fluid force acting on it. The fluid force coefficients are functions of reduced flow velocity $\left(\frac{U}{fd} \right)$. The force

coefficients contain components that are functions of tubes acceleration, velocity and displacement. The UFM has a detailed view of the fluid forces but depend greatly on the empirical data. Tanaka and Takahara [9] have experimentally determined the fluid force coefficients to predict FEI. Semi-analytical approach was proposed by Lever and Weaver [11], in which analytical expression coupling fluid forces and tube motion simplifies the fluid forces. The flow through the arrays was divided into wake and channel regions and it was assumed to be incompressible and one-dimensional. The fluidelastic excitation was considered independent of wake phenomena and the freestream flow was considered along the side of the tube. The flow was modelled using unsteady Bernoulli equation. A time lag was introduced due to a phase lag between tube motion and fluid force. A computational fluid dynamic model was proposed by Hassan et al. [10] to predict the parameter of fluid forces used in modelling FEI. This approach made it possible to bring certain amount of accuracy to the theoretical models. Inviscid fluid flow model is discussed in the work of Dalton and Helfinstine [8] in which the problem of an accelerating potential flow past an array of cylindrical tubes using method of images. Inertial and lift coefficients are predicted for different cylinder arrangements according to this model.

1.2 Problem definition

In this thesis, we use the theory developed in [3] to analyze FEI and post FEI nonlinear dynamics of heat exchanger tubes with loose support and initial axial load. As mentioned in [13], increase in the initial axial load may lead to buckling instability when the fluid flow velocity crosses the critical value. Moreover, the effect of non-linearity induced due to loose support and induced axial tension is also investigated. The heat-exchanger tubes are modelled as a simply supported beam. A mathematical model of a single flexible cylinder in an array of rigid cylinders with a loose support at the beam midspan subjected to cross-flow and initial axial load is developed. Stability and bifurcation analysis of the system is performed by comparing with an heatexchanger tube without loose support.

1.3 Thesis structure

The entire thesis paper is formatted in five chapters dealing with fluid structural interaction of heat-exchanger tubes. The first chapter covers introduction: the various mechanisms involved in the vibration caused due to fluid structural interaction were discussed. On the basis of the literature survey, it was found that fluidelastic instability was the main cause of vibration in heat-exchanger tubes. In the second chapter, various forces acting on the cylinders were studied, an expression for the lift force acting on the heat-exchanger tubes is derived on the basis of Quasi-steady model. In the third chapter, the physical system is analytically modelled to find the governing equation of motion. The governing equation is transformed into a set of five delay differential equation using Galerkin approximation and modal truncation technique. The numerical results are obtained by solving these DDEs are discussed in the fourth chapter. The linear and non-linear model were separately analysed and stability charts and bifurcation diagrams were plotted. Finally we conclude the thesis in the fifth chapter.

Chapter 2

The flow-induced forces on a flexible tube

The fluidelastic instability analysis employed in the present work is based on the ‘‘Quasi-steady’’ model proposed by Price and Paidousiss [3] which is similar to the quasi-static model [16] with an addition of one important frequency-dependent term introduced by Simpson and Flower [19]. In this approach the cylinder under consideration is assumed to be flexible while the other cylinders in the array to be rigid. It is assumed that the cylinder is being provided with a system flexibility by an orthogonal spring system supporting the cylinder (see Fig. 2.1). The equation of motion of the system is written as:

$$[M] \ddot{z} + [C] \dot{z} + [E] z = F \quad (2.1)$$

Here; $[M] = ml [I_2]$, where m is the mass per unit length and l is the tube length; $[C] = c [I_2]$ is the mechanical damping matrix, where c is the equivalent modal viscous damping coefficient; $[E] = K [I_2]$, where K is the equivalent modal stiffness; $z = [x, y]^T$, where x and y are the displacement along and perpendicular to the direction of flow.

2.1 Fluid forces and flow retardation

Quasi-static analysis [19] predicts the force in x and y direction due to fluid flow as:

$$F_x = \frac{1}{2} \rho U_\infty^2 l d \left(C_D \left[1 - \frac{2}{U_\infty a} \dot{x} \right] + C_L \frac{\dot{y}}{U_\infty a} \right) \quad (2.2)$$

$$F_y = \frac{1}{2} \rho U_\infty^2 l d \left(C_L \left[1 - \frac{2}{U_\infty a} \dot{y} \right] + C_D \frac{\dot{x}}{U_\infty a} \right) \quad (2.3)$$

where ρ is the fluid density, a is the ratio between the flow velocity impinging on the cylinder and free stream velocity (U_∞); $a = T / (T - \frac{1}{2}d)$, where C_L and C_D are respectively the lift and drag coefficients which can be expressed in linear form as:

$$C_L = C_{L0} + x \frac{\partial C_L}{\partial x} + y \frac{\partial C_L}{\partial y} \quad (2.4)$$

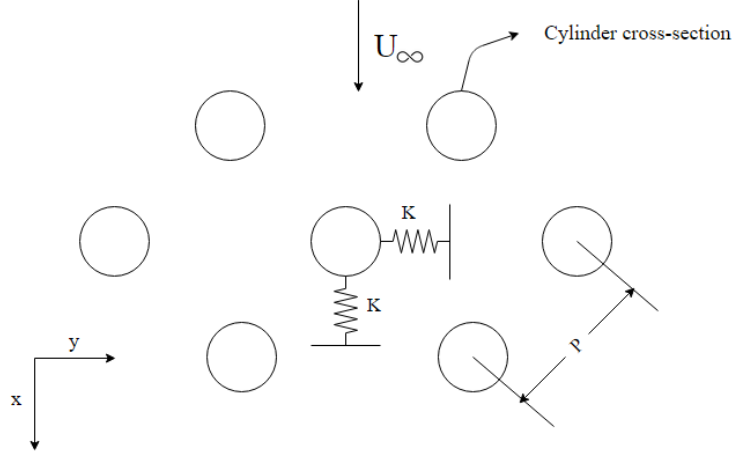


Figure 2.1: Schematic of the orthogonal spring system used to represent cylinder flexibility, where P is the pitch of the array and U_∞ is the flow velocity

$$C_D = C_{D0} + x \frac{\partial C_D}{\partial x} + y \frac{\partial C_D}{\partial y} \quad (2.5)$$

The flow approaches the cylinder at a retarded velocity instead of constant velocity (i.e, $U < U_\infty$) and it impinge on the cylinder at a time t . Now if the fluid flow was steady, it would have impinged on the cylinder at an earlier time $(t - \Delta t)$. Since we consider a constant flow velocity for the entire analysis a time delay is introduced in cylinder displacement as $x(t - \Delta t)$ and $y(t - \Delta t)$. This is particularly important when there is a large changes in the fluid force coefficients with small change in cylinder displacements, especially for motion in the y -direction. If the fluid flow velocity (U) impinging on the cylinder is constant, then the time taken by the fluid to flow from $x = x_1$ to $x = R + \Delta R$ is:

$$t = \frac{(x_1 - R - \Delta R)}{U} \quad (2.6)$$

where, R is the radius of the tube. When the fluid flow approaches near to tube stagnation point, the velocity gets retarded. Now if the approach velocity is taken as varying velocity, U_{appr} , then the traverse time is calculated as:

$$t + \Delta t = \int_{R+\Delta R}^x \frac{1}{U_{appr}} dx \quad (2.7)$$

use potential flow theory around an isolated cylinder, $U_{appr} = U (1 - R^2/x^2)$, we get:

$$\Delta t = \frac{R}{2U} \left[\ln \left(\frac{x_1 - R}{x_1 + R} \right) - \ln \left(\frac{\Delta R}{2R + \Delta R} \right) \right] \quad (2.8)$$

It has been assumed that x_1 very large when compared with ΔR [19], the expression Eq. (2.8) is reduced to

$$\Delta t = \frac{R}{2U} \ln \left(\frac{2R}{\Delta R} \right) \quad (2.9)$$

For a specific value of ΔR , one may write the above expression as

$$\Delta t = \mu \frac{D}{U} \quad (2.10)$$

for a square array, if pitch to diameter ratio is $P/D = 1.5$ then the coefficient $\mu = 1$ [4]. If the cylinder motion is in damped harmonic form, apparent displacement $\Delta y = y(t) - y(t + \Delta t)$ occurred due to flow retardation, it can be expressed as:

$$\Delta y = y(t)(1 - \tilde{g}) \quad (2.11)$$

where $\tilde{g} = \exp(-\lambda\mu d/U)$. The velocity with which fluid impinges the cylinder except the ones in the upstream row is $U = aU_\infty$. Consider the retardation effect in Eq. (2.4) and Eq. (2.5), we get:

$$C_L = C_{L0} + \tilde{g} \left(x \frac{\partial C_L}{\partial x} + y \frac{\partial C_L}{\partial y} \right) \quad (2.12)$$

$$C_D = C_{D0} + \tilde{g} \left(x \frac{\partial C_D}{\partial x} + y \frac{\partial C_D}{\partial y} \right) \quad (2.13)$$

Substituting these expressions in Eq. (2.1), we get,

$$F = \frac{1}{2}\rho U_\infty^2 l d \left\{ \frac{1/2\pi d}{U_\infty^2} [A] \ddot{z} + \frac{1}{U_\infty a} [B] \dot{z} + \tilde{g} K z + F_0 \right\} \quad (2.14)$$

where, $[A]$ is the added mass matrix, $[B]$ is the fluid damping matrix, $[K]$ is the fluid stiffness matrix.

$$[B] = \begin{bmatrix} -2C_{D0} & C_{L0} \\ -2C_{L0} & -C_{D0} \end{bmatrix}$$

$$[K] = \begin{bmatrix} \frac{\partial C_D}{\partial x} & \frac{\partial C_D}{\partial y} \\ \frac{\partial C_L}{\partial x} & \frac{\partial C_L}{\partial y} \end{bmatrix}$$

$$[F_0] = \begin{bmatrix} C_{D0} \\ C_{L0} \end{bmatrix}$$

For a symmetrically positioned single flexible tube with respect to the adjacent cylinders,

$$C_{L0} = \frac{\partial C_L}{\partial x} = \frac{\partial C_D}{\partial x} = 0 \quad (2.15)$$

For a cross flow, the instability is mainly because of lift forces and the contribution of drag force on instability is less. From Eq. (2.14), the force component along the direction of lift can be written as

$$F_L = -\frac{\pi}{4}\rho L D^2 C_{ma} \ddot{y} - \frac{1}{2a}\rho U_\infty L C_{D0} \dot{y}(t) + \frac{1}{2}\rho U_\infty^2 L D \frac{\partial C_L}{\partial y} y(t - \Delta t) \quad (2.16)$$

In an upstream-cylinder a must be unity, because the approach velocity is U_∞ . Therefore, we take $U_\infty = U_G = U$. Hence, the lift force F acting on a flexible tube, surrounded by several rigid tubes, under cross flow can be written as follows:

$$F_L = -\frac{\pi}{4}\rho L D^2 C_{ma} \ddot{y} - \frac{1}{2}\rho U L C_{D0} \dot{y}(t) + \frac{1}{2}\rho U^2 L D \frac{\partial C_L}{\partial y} y(t - \Delta t) \quad (2.17)$$

Chapter 3

Mathematical modelling

The system under consideration consists of a square inline cylinder array under cross-flow subjected to an external initial axial load (P_0) as shown in Fig. 3.1. In this work, the flexible tube is assumed as Euler–Bernoulli beam, the end support is assumed to be simply supported and the middle support (baffle) is assumed to be loose support. Based on the above assumptions, the mathematical model of the flexible cylinder is given as:

$$EI \frac{\partial^4 w}{\partial x^4} + c \frac{\partial w}{\partial t} + m \frac{\partial^2 w}{\partial t^2} - \frac{EA}{2L} \frac{\partial^2 w}{\partial x^2} \int_0^L \left(\frac{\partial w}{\partial t} \right)^2 dx + P_0 \frac{\partial^2 w}{\partial x^2} + \delta(x - x_b) f(w) = F(w, \dot{w}, \ddot{w}) \quad (3.1)$$

where, EI is the flexural rigidity, C is the damping coefficient, A is the area of cross-section of the cylindrical tube, and w is the transverse displacement. P_0 represents the initial axial load, F is the cross-flow induced force acting on the cylinder and f is the force due to the loose support constraint, $\delta(x - x_b)$ represents the dirac delta function with x_b being the loose support constraint location. Also, throughout the study it is assumed that the loose support is symmetrically attached to the cylindrical beam, i.e., ($\xi_b = 0.5$). The expression for cross-flow induced force F is given by:

$$F = M \frac{\partial^2 w(x, t)}{\partial t^2} + B \frac{\partial w(x, t)}{\partial t} + C w(x, t - \Delta t)$$

where,

$$M = -\frac{\pi}{4} \rho D^2 C_{ma} \quad B = -\frac{1}{2} \rho U D C_D \quad C = \frac{1}{2} \rho U^2 D \frac{\partial C_L}{\partial w} \quad \Delta t = \mu \frac{D}{U}$$

Here D denotes the diameter of the cylinder, and ρ and U are the fluid density and velocity respectively. C_d and C_L are the drag and lift coefficients which depends on the gap flow velocity (flow velocity in the gap between the cylinders). C_{ma} is the virtual or added mass coefficient of the fluid around the cylinder, μ is a parameter which relates to the array pattern and Δt is the time delay which arises due to phase lag between cylinder motion and fluid dynamic forces.

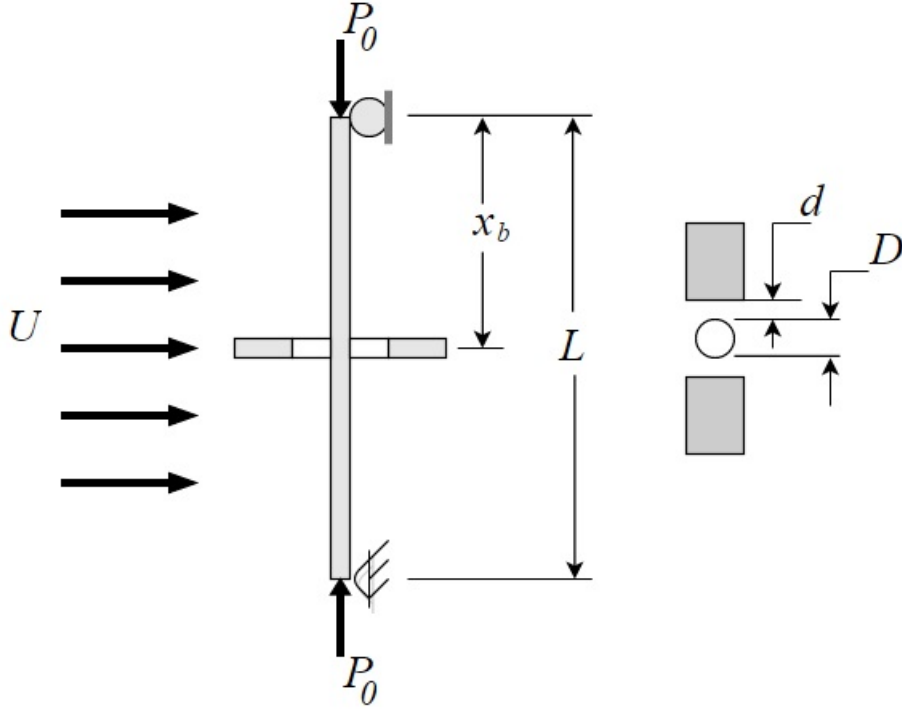


Figure 3.1: Schematic of the system

We now introduce the following non-dimensional quantities:

$$\begin{aligned}
 \eta &= \frac{w}{D}, & \xi &= \frac{x}{L}, & \tau &= \lambda_1^2 \sqrt{\frac{EI}{mL^4}} t = \Omega_1 t, & \zeta &= \frac{c}{\Omega_1 m}, \\
 \tilde{m} &= \frac{m}{\rho D^2}, & \tilde{U} &= \frac{2\pi U}{D\Omega_1}, & p_0 &= \frac{P_0 L^2}{EI}, & \beta &= \frac{1}{1 + 4\tilde{m}/\pi C_{ma}}, \\
 \gamma &= \frac{AD^2}{2I\lambda_1^2}, & \tilde{f} &= \frac{f}{m\Omega_1^2}
 \end{aligned}$$

The variable λ_1 denotes the dimensionless eigenvalue of the first mode for a simply supported beam. Substituting the non-dimensional parameters in Eq. (3.1) yields:

$$\begin{aligned}
 & \frac{1}{1-\beta} \frac{\partial^2 \eta(\xi, \tau)}{\partial \tau^2} + \left(\zeta + \frac{\tilde{U} C_D}{4\pi \tilde{m}} \right) \frac{\partial \eta(\xi, \tau)}{\partial \tau} + \frac{1}{\lambda_1^4} \frac{\partial^4 \eta(\xi, \tau)}{\partial \xi^4} + \frac{1}{\lambda_1^4 p_0} \frac{\partial^2 \eta(\xi, \tau)}{\partial \xi^2} \\
 & - \gamma \frac{\partial^2 \eta(\xi, \tau)}{\partial \eta^2} \int_0^1 \left(\frac{\partial \eta(\xi, \tau)}{\partial \xi} \right)^2 d\xi - \frac{\tilde{U}^2}{8\pi^2 \tilde{m}} \frac{\partial C_L}{\partial \eta} \eta(\xi, \tau - T) + \delta(\xi - \xi_b) \tilde{f}(\eta) = 0
 \end{aligned} \tag{3.2}$$

Equation (3.2) is a second order PDE, with time delay terms. The dimensionless time delay (T) is taken as $2\pi/\tilde{U}$ for $\mu = 1$ [4]. We now use modal truncation techniques and Galerkin approximation to discretize the PDE (3.2) into a set of finite ODEs. The solution $\eta(\xi, \tau)$ of Eq. (3.2) is therefore

approximated using a series solution as:

$$\eta(\xi, \tau) = \sum_{j=1}^N \phi_j(\xi) q_j(\tau) \quad (3.3)$$

where $\boldsymbol{\phi} = [\phi_1, \phi_2, \dots, \phi_N]^T$ are the basis functions and $\mathbf{q} = [q_1(\tau), q_2(\tau), \dots, q_N(\tau)]^T$ are the time dependent coefficients. We use an orthogonal set of basis functions to take the advantage of the properties of orthogonal functions. Also, a five mode expansion is used in the analysis ($N = 5$), that is justifiable due to the fact that the system response is dominated mainly by the first few modes.

Now on substituting Eq. (3.3) into Eq. (3.2), post-multiplying by $\phi_i(\xi)$ and integrating the resultant expression from 0 to 1 gives:

$$\begin{aligned} \frac{1}{1-\beta} \int_0^1 \frac{\partial^2}{\partial \tau^2} (\sum \phi_j q_j) \phi_i d\xi + \left(\zeta + \frac{\tilde{U} C_D}{4\pi \tilde{m}} \right) \int_0^1 \frac{\partial}{\partial \tau} (\sum \phi_j q_j) \phi_i d\xi + \frac{1}{\lambda_1^4} \int_0^1 \frac{\partial^4}{\partial \xi^4} (\sum \phi_j q_j) \phi_i d\xi \\ + \frac{p_0}{\lambda_1^2} \int_0^1 \frac{\partial^2}{\partial \xi^4} (\sum \phi_j q_j) \phi_i d\xi - \gamma \int_0^1 \left(\frac{\partial^2}{\partial \xi^2} (\sum \phi_j q_j) \phi_i \int_0^1 \left(\frac{\partial}{\partial \xi} (\sum \phi_j q_j) \right) d\xi \right) d\xi \\ - \int_0^1 \frac{\tilde{U}^2}{8\pi^2 \tilde{m}} \frac{\partial C_L}{\partial \eta} (\sum q_j(\tau - T) \phi_j) \phi_i d\xi + \int_0^1 \delta(\xi - \xi_b) \tilde{f} (\sum q_j(\tau - T) \phi_j) \phi_i d\xi = 0 \end{aligned} \quad (3.4)$$

The orthogonality of eigenfunction, $\phi_i(\xi)$, yields the following:

$$\int_0^1 \phi_j \phi_i d\xi = \begin{cases} 1 & \text{if } i = j \\ 0 & \text{if } i \neq j \end{cases} \quad \int_0^1 \frac{\partial^2 \phi_j}{\partial \xi^2} \phi_i d\xi = \begin{cases} -\lambda^2 & \text{if } i = j \\ 0 & \text{if } i \neq j \end{cases} \quad (3.5)$$

$$\int_0^1 \frac{\partial^4 \phi_j}{\partial \xi^4} \phi_i d\xi = \begin{cases} \lambda^4 & \text{if } i = j \\ 0 & \text{if } i \neq j \end{cases} \quad (3.6)$$

also

$$\int_0^1 \delta(\xi - \xi_b) \tilde{f} (\sum \phi_j(\xi) q_j) \phi_i d\xi = \tilde{f}(\eta_b) \phi_i(\xi_b) \quad (3.7)$$

Since all the variables are dimensionless, we drop the tildes ($\tilde{\cdot}$) over U , m and f . Exploiting the orthogonal relationships (Eq. (3.5)–(3.7)) in Eq. (3.4), yields:

$$\begin{aligned} \frac{1}{1-\beta} \ddot{q}_i(\tau) + \left(\frac{\delta_i v_i}{\pi} + \frac{U C_D}{4\pi m} \right) \dot{q}_i(\tau) + v_i^2 \left[1 - \frac{p_0}{\lambda_i^2} \right] q_i(\tau) + \gamma b_{ii} \left(\sum_{j=1}^N q_j^2(\tau) b_{jj} \right) q_i(\tau) \\ - \frac{U^2}{8\pi^2 m} \frac{\partial C_L}{\partial \eta} q_i(\tau - T) + f(\eta_b) \phi_i(\xi_b) = 0 \end{aligned} \quad (3.8)$$

where $v_i = (\lambda_i/\lambda_1)^2$ is the ratio of i^{th} non-dimensional natural frequency to the first non-dimensional frequency of simply supported beam, and the viscous damping (ζ) is replaced by the modal damping

$\delta_i v_i / \pi$. The coefficient b_{ii} is the diagonal elements of matrix B , that is evaluated as:

$$B = \int_0^1 \phi \phi''^T d\xi = - \int_0^1 \phi' \phi'^T d\xi$$

where $\phi = [\phi_1, \phi_2, \dots, \phi_N]^T$; ϕ' and ϕ'' are respectively the first and second derivatives with respect to ξ .

For a square array with pitch-to-diameter ratio as 1.5, the numerical values of various parameters in Eq. (3.8) are $\beta = 0.24$, $\delta_i = 0.06$, $C_D = 0.26$, $m = 0.3$, and $\partial C_L / \partial \eta = -8.1$. The restraining force f in Eq. (3.8) arises due to the loose support constraint. In this work, we have first modeled the loose support as a cubic spring as follows:

$$f(\eta_b) = \kappa \eta_b^3 \quad (3.9)$$

where κ is the stiffness of the cubic spring. The value of the spring stiffness κ is taken as 1000 [4]. Modeling of loose support as a cubic spring is analytically useful and aids in the evaluation of poincare maps, etc. However, a more physically realistic way of modeling loose support is by using a tri-linear spring in which restraining force is represented by a non analytical function of η_b [4], given by:

$$f(\eta_b) = \kappa \left[\eta - \frac{1}{2} (|\eta + d| - |\eta - d|) \right] \quad (3.10)$$

where $2d$ is the non-dimensionalized gap (with respect to D), between support and cylinder.

Upon using the above force models (Eq. (3.9) and Eq. (3.10)) and integrating the ODEs Eq. (3.8) using Matlab ode solvers we obtain an approximation to the response of the PDE Eq. (3.1). In the next section, we compare the stability and bifurcation diagrams obtained for both force models under different initial axial load conditions.

Chapter 4

Stability and bifurcation analysis

4.1 Stability Analysis

In this section, we analyse stability and bifurcation of the system with various types of loose supports. From Eq. (3.1), it is clear that for sufficiently large P_0 , the destabilizing force $P_0(\partial^2 W/\partial x^2)$ may overcome the restoring flexural force $EI(\partial^4 W/\partial x^4)$, thereby resulting in divergence (buckling) instability, also known as pitchfork (static) bifurcation. On the other hand, the cylinder can also undergo Hopf bifurcation because of the flutter instability due to cross-flow.

The buckling instability and flutter instability are identified from the the critical values of flow velocity (U) and initial axial load (p_0). To determine these critical values, first we linearized the model Eq. (3.8) as follows:

$$\ddot{q}_i(\tau) + (\alpha_1 + \alpha_2 U)\dot{q}_i(\tau) + \alpha_3 \left[1 - \frac{p_0}{\lambda_1^2}\right] q_i(\tau) + \alpha_4 U^2 q_i(\tau - T) = 0 \quad (4.1)$$

where $\alpha_1 = 0.0145v_i$, $\alpha_2 = 0.00524$, $\alpha_3 = 0.76v_i^2$, and $\alpha_4 = 0.026$. For stability analysis, we equate the non-linear constraint force $f(\eta_b)$ to zero. We now assume the solution of the Eq. (4.1) as:

$$q_i = q_{i0} e^{j\omega_i t} \quad (4.2)$$

where, ω_i is the i^{th} dimensionless eigenfrequency of the beam and $j = \sqrt{-1}$. Substituting Eq. (4.2) in Eq. (4.1) yields:

$$-\omega_i^2 + (\alpha_1 + \alpha_2 U)j\omega_i + \alpha_3 \left[1 - \frac{p_0}{\lambda_i^2}\right] + \alpha_4 U^2 e^{-j\omega_i T} = 0 \quad (4.3)$$

We now substitute $e^{-j\omega_i T} = \cos \omega_i T - j \sin \omega_i T$ in Eq. (4.3) and equate the real and imaginary parts to zero, we get:

$$-\omega_i^2 + \alpha_3 \left[1 - \frac{p_0}{\lambda_i^2}\right] + \alpha_4 U^2 \cos \omega_i T = 0 \quad (4.4)$$

$$(\alpha_1 + \alpha_2 U)\omega_i + \alpha_4 U^2 \sin \omega_i T = 0 \quad (4.5)$$

At the onset of flutter instability (i.e. at Hopf bifurcation), the critical flow velocity (U) assumes

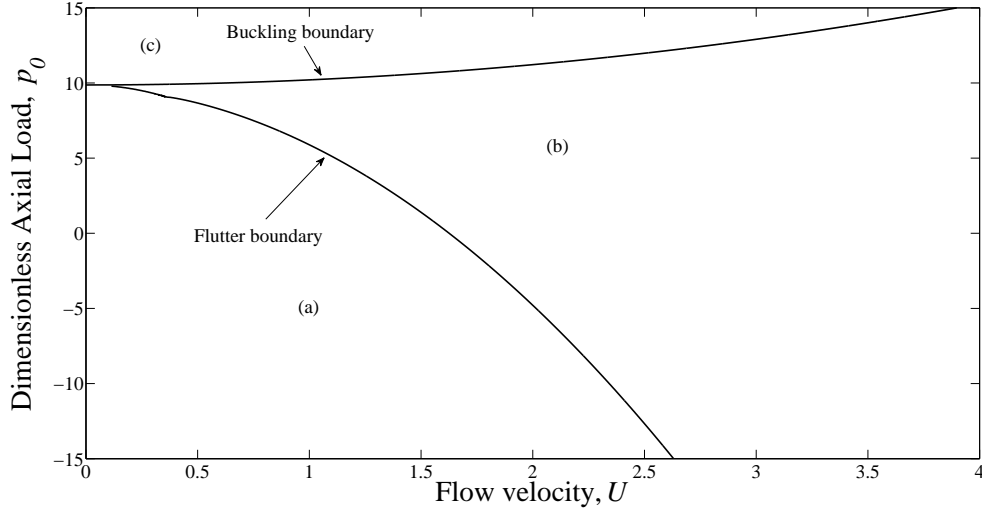


Figure 4.1: Sketch of stability regions

the value U_H , and therefore the Eq. (4.4) and Eq (4.5) become:

$$-\omega_i^2 + \alpha_3 \left[1 - \frac{p_0}{\lambda_i^2} \right] + \alpha_4 U_H^2 \cos \omega_i T = 0 \quad (4.6)$$

$$(\alpha_1 + \alpha_2 U_H) \omega_i + \alpha_4 U_H^2 \sin \omega_i T = 0$$

The critical flow velocity U_H and the dimensionless eigenfrequency ω_i can be obtained from Eq. (4.6) at different axial load p_0 . At Hopf bifurcation the value of ω_i must be purely real. We now discuss the buckling instability, a case of static bifurcation which occurs when the initial axial load (p_0) assumes a large value, say p_{os} . The load p_{os} which is also known as the critical axial load, that is obtained by substituting $\omega_i = 0$ in Eq. (4.3), that implies:

$$\alpha_3 \left[1 - \frac{p_0}{\lambda_i^2} \right] + \alpha_4 U^2 = 0 \quad (4.7)$$

The above expression Eq. (4.7) tells the critical axial load p_{os} for different values of the flow velocity. We now vary the flow velocity (U) and the initial axial load (p_0) in Eq. (4.4) and Eq. (4.5) to obtain a sketch of the stability regions in the plane of (U, p_0) as shown in Fig. 4.1. It has been found that the stability boundaries divide the diagram Fig. 4.1 into three regions marked as (a), (b) and (c).

- Region (a): Smaller values of U and p_0 gives a stable equilibrium.
- Region (b): Smaller value of U and larger value of p_0 results in buckling instability
- Region (c): Larger value of U and smaller value of p_0 leads to flutter instability

Thus, the stability diagram obtained in this section helps to identify the flutter and buckling instability boundaries. However, this stability analysis is based on a linearized model of Eq. (4.1) and

does not take into account the inherent nonlinearities present in the system. Moreover for predicting the post-instability behavior accurately, the nonlinearities must be taken into consideration. We therefore include the loose constraint and the axial deformation nonlinearities and study the associated bifurcation diagrams. It should be particularly noted that, apart from the flutter instability the effect of buckling due to axial load leads to pitchfork bifurcation.

4.2 Bifurcation Analysis

Bifurcation diagrams helps to understand the complete dynamics of the system. They allow us to pin-point the sudden changes in the system behavior and helps to determine whether the system is chaotic or not. We now use the nonlinear model Eq. (3.8) to obtain the bifurcation diagrams. As discussed in the previous Chapter 3, we are considering the nonlinearity in our model due to loose support constraint conditions and initial axial load conditions (p_0).

To analyze the complete behavior of the system, the nonlinear force due to the loose support is modeled using cubic and trilinear spring and the initial axial load (p_0) is varied from compressive to tensile. We perform the simulations for the following load conditions; $p_0 = -15$, $p_0 = 0$, $p_0 = 9$ and $p_0 = 15$, where the negative sign indicates tensile loading.

Applying the various initial axial load conditions and the various force model, we integrate the DDEs forward in time and obtain the bifurcation plots when the system reaches the steady state condition. The initial conditions for all the cases were assumed as $q_i = 0.001$, $\dot{q}_i = 0$ along with the parameter $\gamma = 0.015$ [13]. All the simulations were performed using Matlab dde solver “dde23” with tolerances, AbsTol= $1e^{-3}$ and RelTol= $1e^{-6}$. In the upcoming sections, section (4.2.1) and section (4.2.2) we study the stability and bifurcation of the system with the different loose support models.

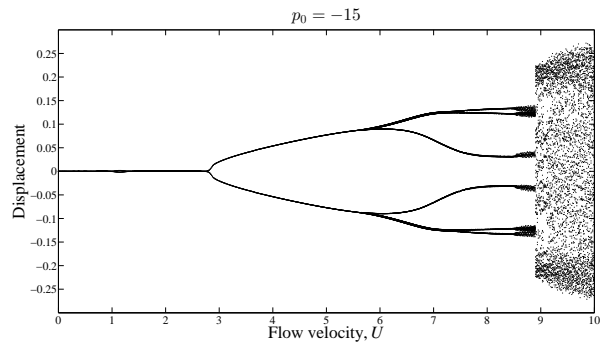
4.2.1 Cubic Spring model

In this section, we model the loose support as cubic spring, then we analyse the bifurcation and the stability of the system at various initial axial load and flow velocity. The cubic spring model is defined as:

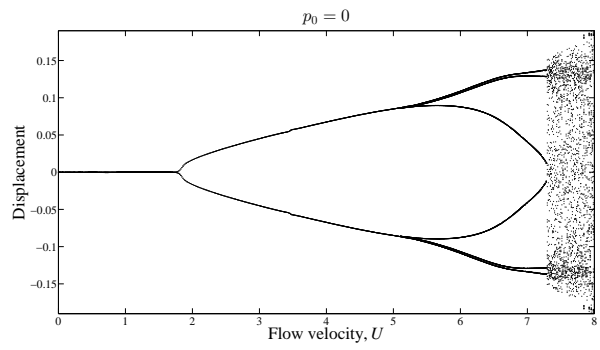
$$f(\eta_b) = \kappa\eta_b^3 \quad (4.8)$$

where κ is the stiffness of the spring and η_b is the loose support location. The value of the spring constant is assumed to be $\kappa = 1000$. Substitute the above expression of the loose support constraint force Eq. (4.8) in to the ODEs (see Eq. (3.8)), then integrate resulting ODEs to obtain the system response. The bifurcation diagrams (see Fig. 4.2) corresponds to the steady state displacement amplitude, that is obtained by integrating the system for a very long time and considering the displacement amplitude only for the last 100 time units.

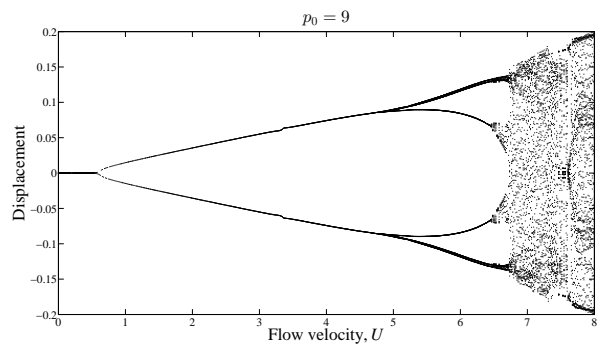
Figure 4.2 shows the displacement amplitude at the loose support ($\zeta = 0.5$) by varying flow velocity (U) at different initial axial load (p_0) conditions. We can clearly see that the system exhibits post instability bifurcation and chaotic motions for all the load conditions. For all the initial axial load conditions at critical flow velocities, the system undergoes Hopf bifurcation due to flutter instability, except for the case of $p_0 = 15$, where the system undergoes pitchfork bifurcation due to buckling instability.



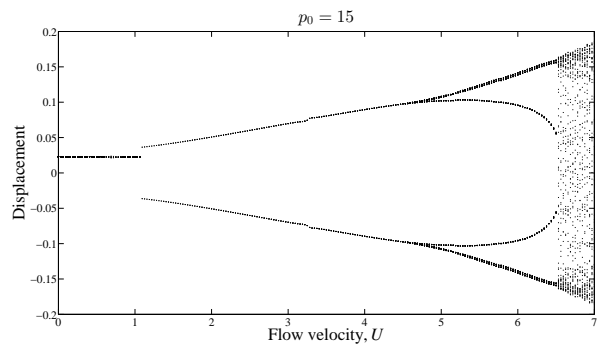
(a)



(b)

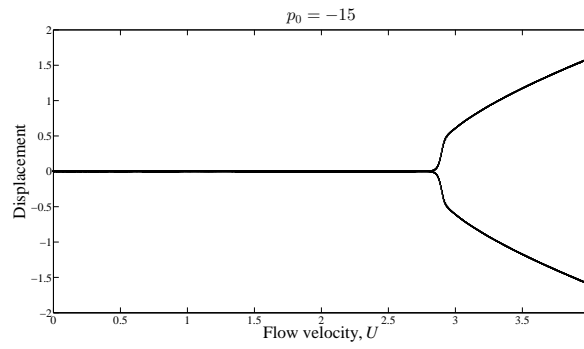


(c)

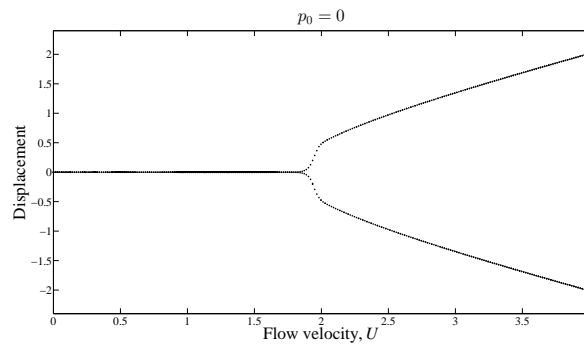


(d)

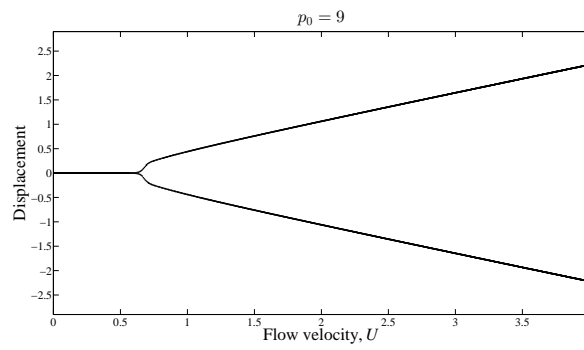
Figure 4.2: Bifurcation diagram of the system with loose support in the middle for different values of initial axial load $p_0 = -15, p_0 = 0, p_0 = 9, p_0 = 15$ is given in figure (a), (b), (c) and (d) respectively



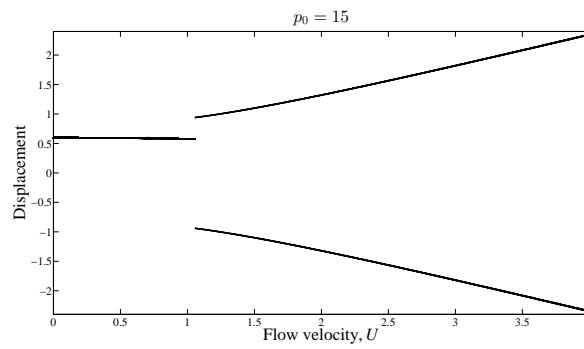
(a)



(b)



(c)



(d)

Figure 4.3: bifurcation diagram of the system with loose support in the middle for different values of initial axial load $p_0 = -15, p_0 = 0, p_0 = 9, p_0 = 15$ is given in figure (a), (b), (c), and (d) respectively

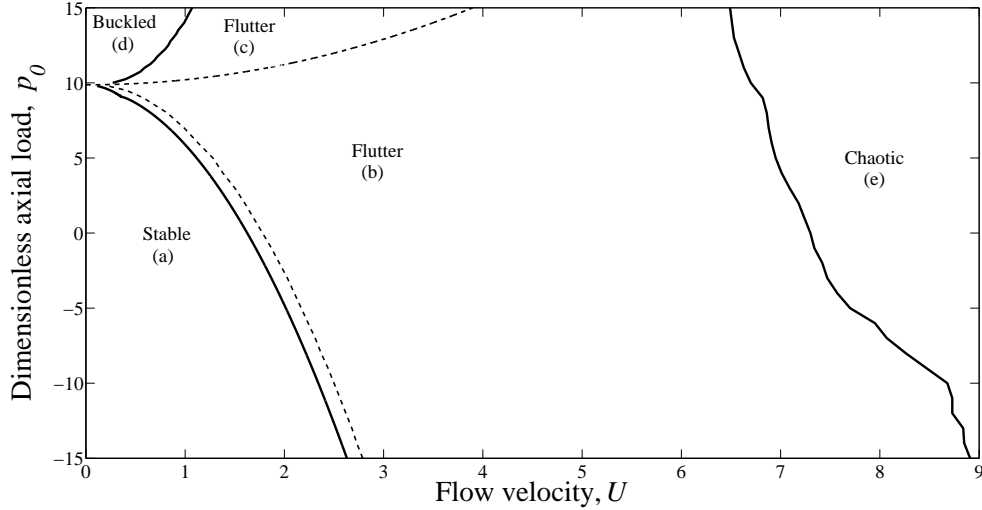


Figure 4.4: Sketch of stability regions with cubic spring support

From Fig. 4.2, we approximately determine the critical flow velocity at instability, at post instability bifurcation, and at chaotic motions. The approximated critical velocities have been shown in Table 4.1. We found that for load condition $p_0 = 15$, the critical flow velocity for instability (U_1) is much lesser when compared with that of the linearized model. Figure 4.5 and Fig. 4.6 shows the phase and displacement plots for flow velocities $U = 1$ and $U = 3$ respectively. One of the interesting feature has been observed in Fig. 4.6 is that, even though the initial axial load was increased beyond the critical value (P_{os}), system is still remains in stable limit cycle motion and the it does not gravitate to buckled equilibrium position (see Fig. 4.6(h)). So we can divide the buckling region (c) of Fig. 4.1 into two separate regions as shown in Fig. 4.4. In the region (d), the system gravitates towards a buckled equilibrium position and in the regions (b) and (c), it undergoes a stable limit cycle motion. Figure 4.7 shows phase diagrams of the system at different loads portraying chaotic motions for velocity $U > U_{ch}$.

In Fig. 4.4 we compare the stability plots obtained using the nonlinear model with the linearized model. On comparing the bifurcation diagram with Fig. 4.2 (with loose support) with Fig. 4.3 (without loose support), we observe that the velocity at which the system loses stability is same for both cases. However no chaotic motions are present due to the non-linearity of loose support. This shows that the presence of chaotic motions in the system is because of the impacting of cylinder with loose supports. The motion of the cylinder in chaotic region is displayed in Fig. 4.7 using phase diagrams and response plots.

4.2.2 Trilinear Spring model

In the previous section, the system was modelled using cubic spring in which the restraining force was taken as $f(\eta_b) = \kappa\eta_b^3$. Even though this particular model facilitates easy mathematical calculations, physically it is not a realistic model. As we can see that, when cylinder is vibrating inside the gap ($|\eta_b| < d$) the spring force acting on the cylinder is zero and when the cylinder impacts on the loose support ($|\eta_b| > d$) a spring force $\kappa\eta_b$ acts on it. One can express this loose support as a trilinear

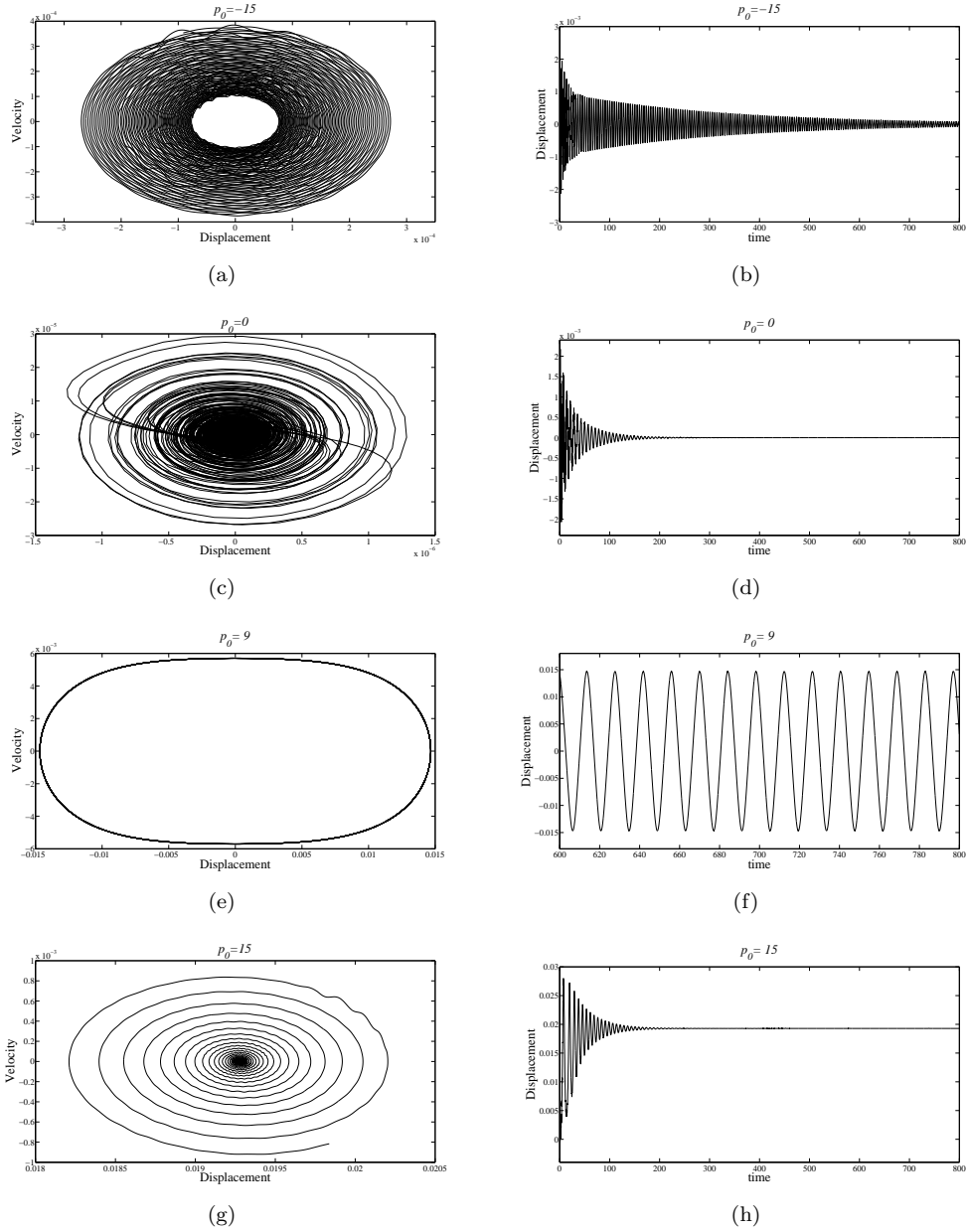
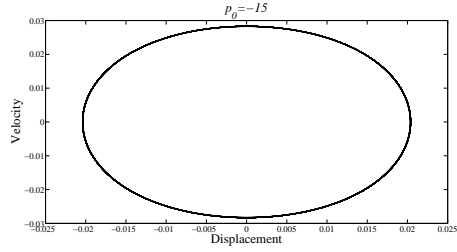
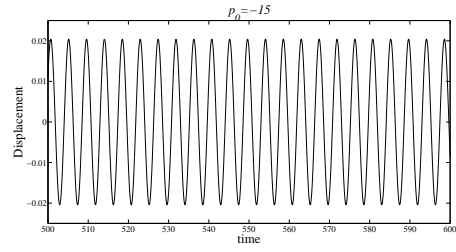


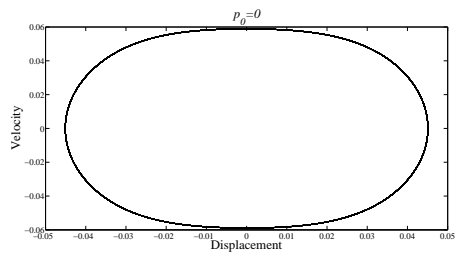
Figure 4.5: Numerical simulations of (4) for $U=1.0$ and different values of p_0



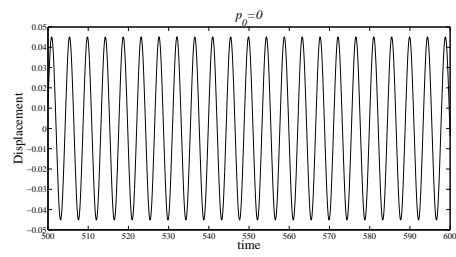
(a)



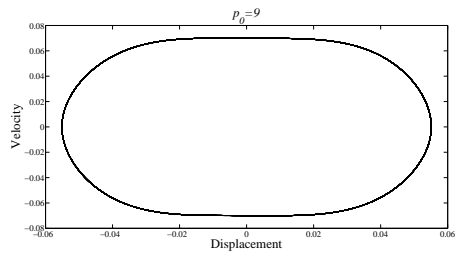
(b)



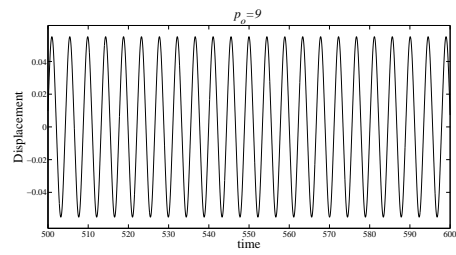
(c)



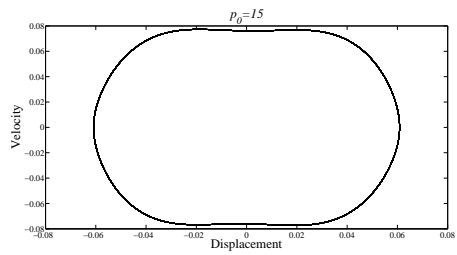
(d)



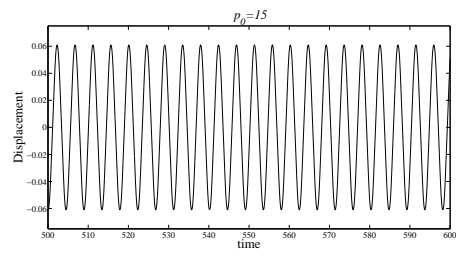
(e)



(f)



(g)



(h)

Figure 4.6: Numerical simulations of (4) for $U=3.0$ and different values of p_0

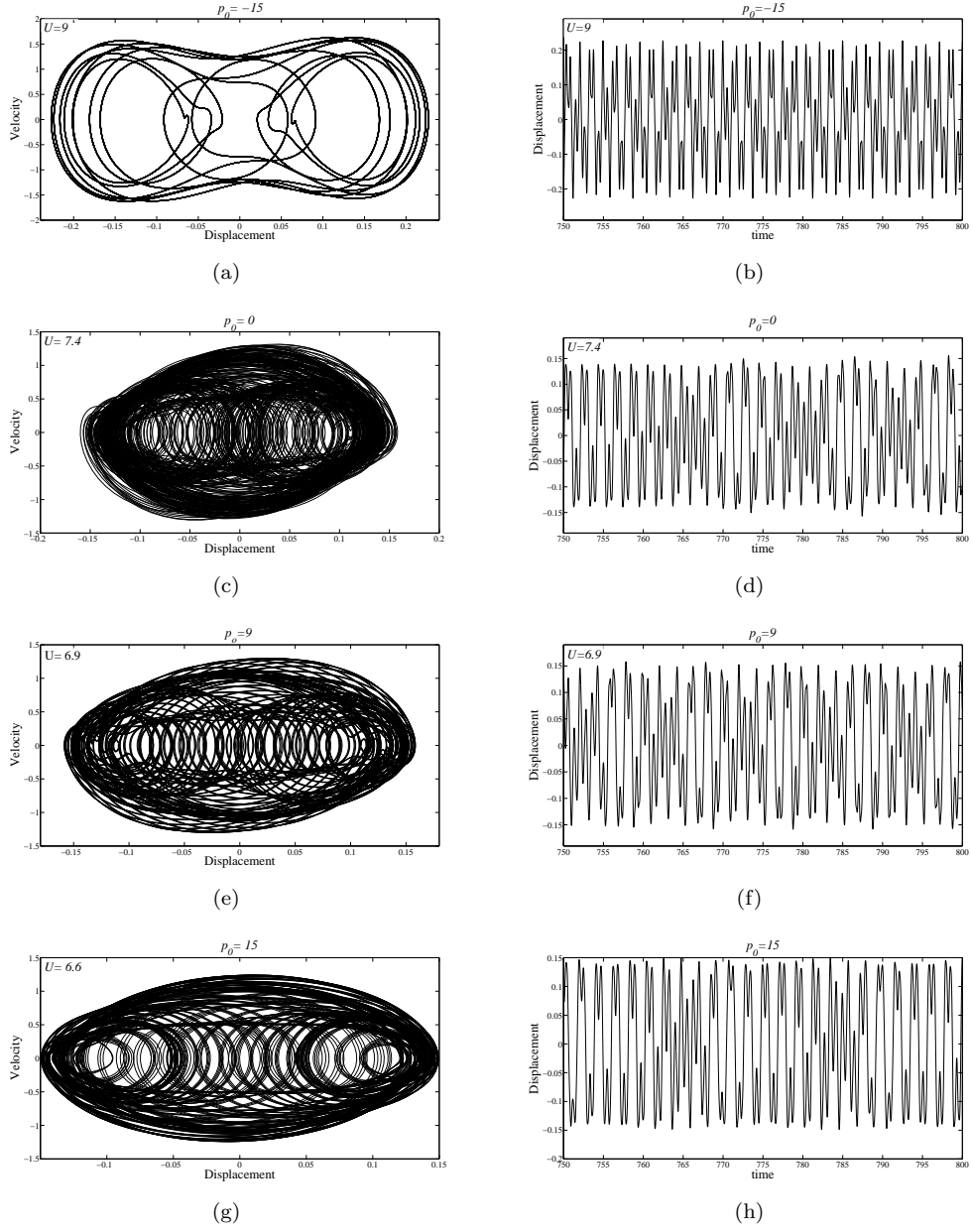


Figure 4.7: Phase diagrams and response plots of the system at different loads, p_0 , portraying chaotic motions for velocity $U > U_{ch}$.

| Axial load | U_1 | U_2 | U_{ch} |
|------------|-------|-------|----------|
| -15 | 2.63 | 5.67 | 8.91 |
| 0 | 1.625 | 5.12 | 7.3 |
| 9 | 0.39 | 4.69 | 6.84 |
| 15 | 1.08 | 4.54 | 6.5 |

Table 4.1: The table shows critical flow velocities for the onset of instability (U_1), velocity corresponding to post-Hopf bifurcation or post-pitchfork bifurcation (U_2) and chaotic motion (U_{ch}) at different axial loads are given below

spring for which the restraining force is given by:

$$f(\eta_b) = \kappa \left[\eta - \frac{1}{2} (|\eta_b + d| - |\eta_b - d|) \right] \quad (4.9)$$

It should be noted that the governing equation is non-analytic when $|\eta| = d$. The value of d is taken as 0.5 as mentioned in [4].

Bifurcation diagrams of the system response for different values of initial axial loads, $p_0 = -15$, $p_0 = 0$, $p_0 = 9$ and $p_0 = 15$ are shown in Fig. 4.8. Table 4.2 shows the critical velocities corresponding to the onset of instability and chaotic motions. From Fig. 4.8(a), bifurcation diagram for $p_0 = -15$, till the flow velocity reaches a value $U = 2.785$, the system is stable and gravitates towards the equilibrium point. When it crosses this critical velocity $U = 2.785$, in the region $2.785 < U < 2.95$, it is having a limit cycle motion. This limit cycle motion is due to the non-linearity due to the effect of deformation induced tension. If the effect of that quantity was neglected or was absent (i.e, $\gamma = 0$), the cylinder would have been suddenly amplified when flow velocity crosses the critical value [12]. It should be noted that the amplitude of the cylinder during this phase is lesser than d , i.e, the cylinder will be vibrating inside the gap. As soon as the cylinder impacts on the loose support, the vibration starts to become chaotic. For $p_0 = -15$, when the flow velocity becomes $U = 2.95$ as the motion become chaotic as shown in Fig. (4.8(a)).

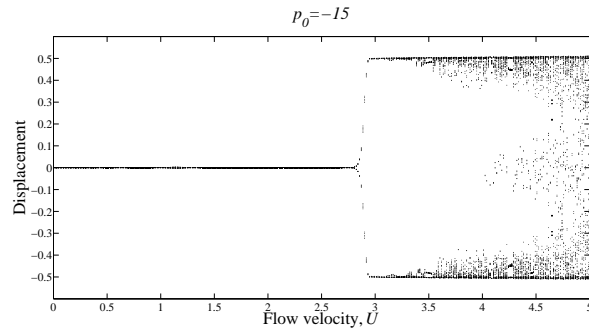
Now, let us take the case when the axial load is $p_0 = 15$, it has been observed that at lesser velocities (when $U < 2.12$) the tube is stable and converging to a stable fixed point steady state condition. Unlike the previous case, this fixed point is shifted from the origin to a buckled position. The amount with which it is displaced from its origin due to buckling is equal to 0.5 (see Fig. 4.8(d)). It is also observed that, as soon as the velocity crosses the value $U = 2.12$ the system becomes chaotic, no limit cycle motion is observed as in the other cases (i.e, for $p_0 = -15$, $p_0 = 0$, $p_0 = 9$). This is probably because the cylinder was already in contact with loose support when it was in buckled equilibrium position and it starts to vibrate chaotically when it just crosses the critical flow velocity $U = 2.12$. Bifurcation diagrams for axial loads $p_0 = 0$ and $p_0 = 9$ are given respectively in Fig. 4.8(b) and Fig. 4.8(c). It is seen that the critical velocities corresponding to Hopf bifurcation and chaotic motion for $p_0 = 0$ are $U_1 = 1.785$ and $U_{ch} = 2.01$ respectively and for $p_0 = 9$ the corresponding critical velocities are $U_1 = 0.583$ and $U_{ch} = 1.1$ respectively.

The time-trace plots and phase diagrams of for the system with loose support modelled as trilinear spring for the flow velocity $U = 1$, at different axial loads $p_0 = -15$, $p_0 = 0$, $p_0 = 9$, and $p_0 = 15$, are shown by Fig. 4.9. Similar to the system modelled with cubic spring, at lower value of initial axial load (P_0) and low fluid flow velocity, the motion of the system gradually gravitates to the the origin due to structural damping 4.9(a) and 4.9(b). At higher loads for the same velocity ($U = 1$),

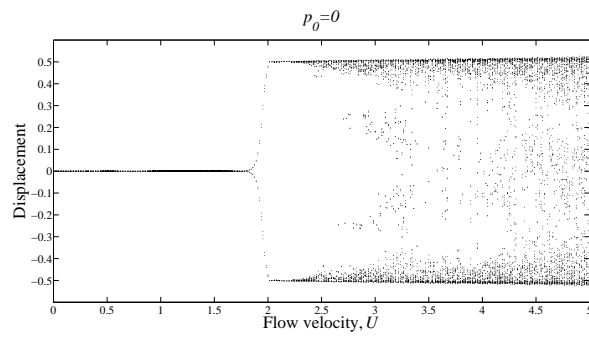
see Fig. 4.9(e) and 4.9(e), the system under goes a limit cycle motion. when the system crosses the critical buckling load corresponding to $U = 1$, it shifts its equilibrium position slightly away from the origin. The system is stable in a buckled position in contact with baffle plate. Figure 4.10 shows chaotic motions of the system at different initial axial load, p_0 when $U > U_{ch}$. It is seen that the amplitude of vibration is does not cross 0.5. That means, the motion of the cylinder is restricted within the baffle gap. The various critical velocities for the onset of instability and chaotic motion of the system at different value of axial loads are given in Table 4.2.

| Axial load | U_1 | U_{ch} |
|------------|-------|----------|
| -15 | 2.785 | 2.95 |
| 0 | 1.785 | 2.01 |
| 9 | 0.583 | 1.1 |
| 15 | — | 2.12 |

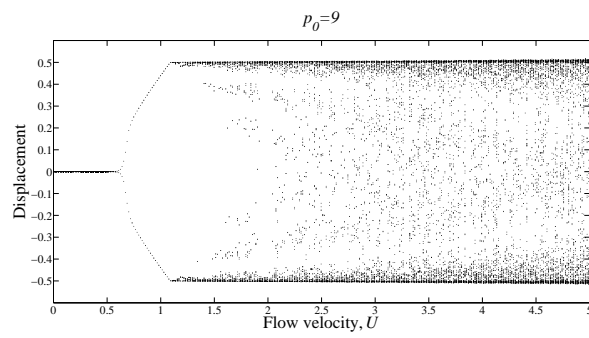
Table 4.2: The table shows critical flow velocities for the onset of instability (U_1) and chaotic motion (U_{ch}) at different axial loads, p_0



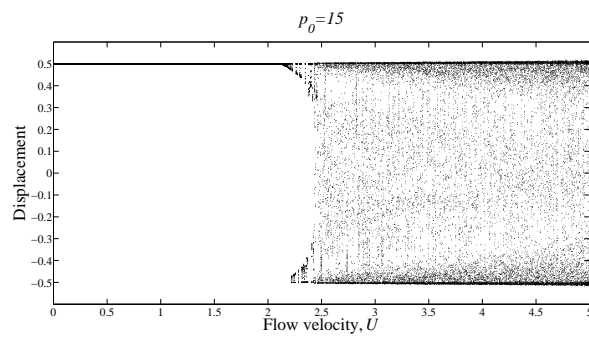
(a)



(b)



(c)



(d)

Figure 4.8: Bifurcation diagram of the system with trilinear spring support in the middle for different values of initial axial load $p_0 = -15, p_0 = 0, p_0 = 9, p_0 = 15$ is given in figure (a),(b),(c) and (d) respectively

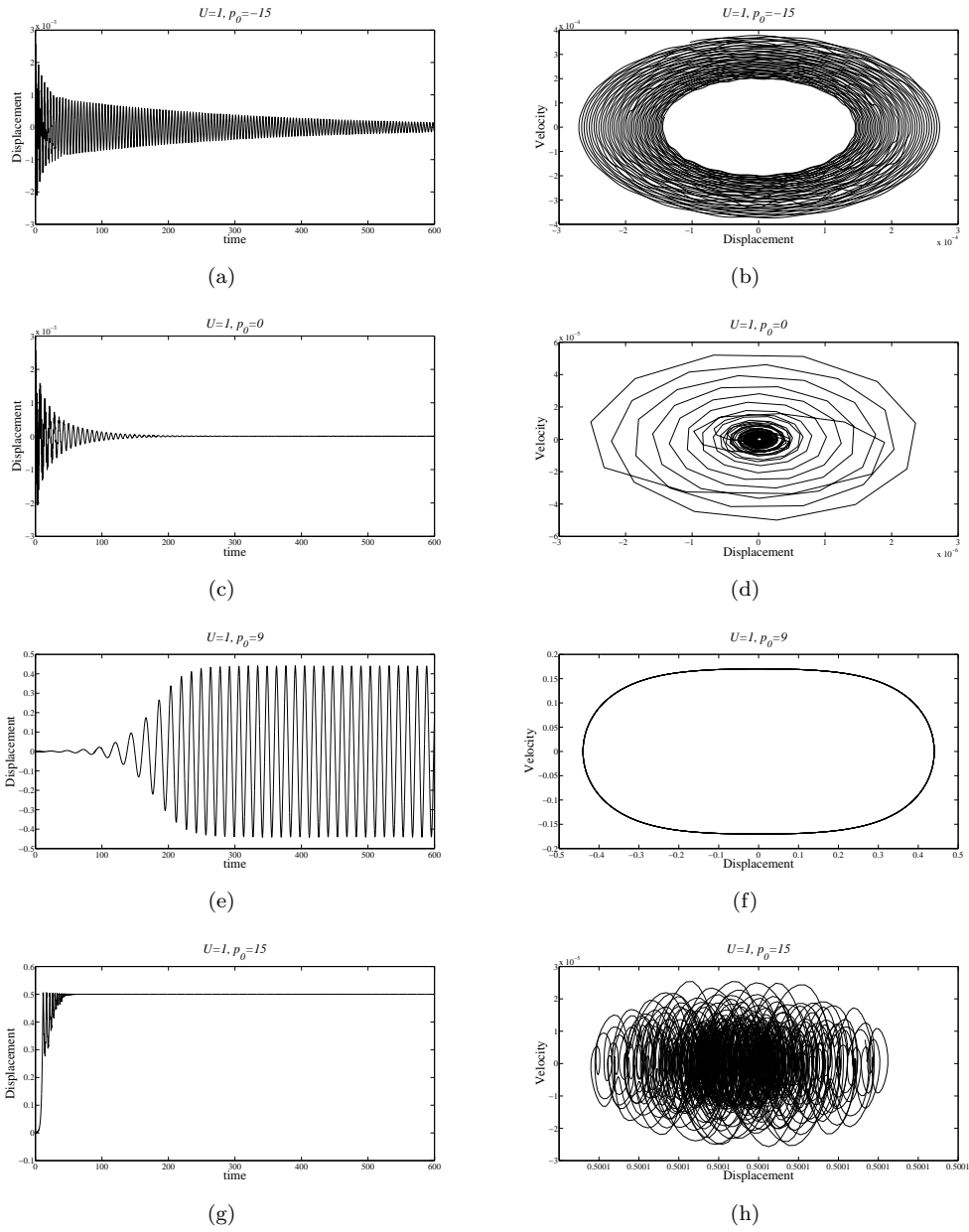


Figure 4.9: Time trace diagram and phase plots of the system when the loose support is modelled as a trilinear spring at different values of initial axial loads, p_0 , for $U = 1$.

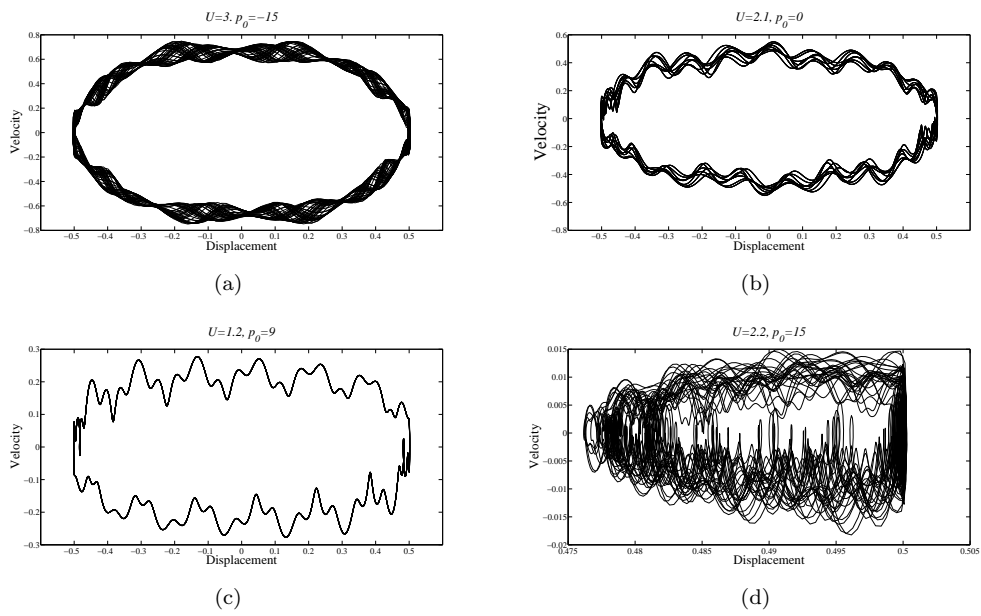


Figure 4.10: Time trace diagram and phase plots of the system when the loose support is modelled as a trilinear spring, at different values of initial axial loads, p_0 , portraying chaotic motions for velocity $U > U_{ch}$.

Chapter 5

Conclusions

In this work we studied the fluidelastic instability of an array of cylindrical tubes with initial axial load and with loose support. A quasi-static approach was employed to analyse the fluidelastic instability of the cylinder for which a single flexible cylinder in the midst of an array of rigid cylinders was taken into consideration. Various forces acting on the tube due to fluid flow has been reviewed. The flow retardation was accounted by introducing a time delay in the motion of the tube while calculating the fluid forces. The loose support was modelled with cubic spring and trilinear spring. The effects of loose support on the stability of the cylindrical array were analyzed by comparing it with a similar system without loose support. The system is modelled analytically by assuming the flexible cylinder as simply supported beam. The model was transformed into a set of second order delay differential equations using Galerkin approximation and modal truncation technique. The obtained system of equation was solved using in built MATLAB solvers.

The study was conducted by analysing the bifurcation diagrams of system at different initial axial loads. It has been found that, non-linearity induced on the tube vibration due to impacting on the loose support leads to chaotic motion, whereas for a system without loose support chaotic motion was absent. The critical flow velocity at which the system starts to amplify the oscillation at the onset of chaotic motions were obtained from the bifurcation diagrams. The instability regions were located using a linearized model of the governing equation and was plotted in a (U, p_0) plane. Stability charts of the system is generated by taking the loose support as cubic and trilinear spring constraints. It has been found that the stability charts for the two non-linear models is deviating from the stability chart of the linearized model. An interesting aspect of this work is that it analyse both the flutter instability and the buckling instability. For higher values of initial axial load, when the fluid flow velocity crosses the critical value, the system loses stability due to buckling which leads to a subcritical pitchfork bifurcation and for lower value of axial loads, system is becomes unstable by flutter instability leading to hopf bifurcation. From the bifurcation diagram of the system in which the loose support modelled as trilinear spring, it can be seen that once the amplitude reaches the “gap distance”, chaotic motions starts and their is no further increase in the amplitude. This suggests that trilinear spring closely resembles the effect of free-gap between the cylinder and the plate.

References

- [1] S.-S. Chen. Flow-induced vibration of circular cylindrical structures. Argonne National Laboratory, 1985.
- [2] S. Ziada. Vorticity shedding and acoustic resonance in tube bundles. *Journal of the Brazilian Society of Mechanical Sciences and Engineering* 28, (2006) 186–189.
- [3] S. Price and M. Paidoussis. A single-flexible-cylinder analysis for the fluidelastic instability of an array of flexible cylinders in cross-flow. *Journal of fluids engineering* 108, (1986) 193–199.
- [4] M. Paidoussis and G. Li. Cross-flow-induced chaotic vibrations of heat-exchanger tubes impacting on loose supports. *Journal of Sound and Vibration* 152, (1992) 305–326.
- [5] B. Roberto. W Low frequency, self-excited vibration in a row of circular cylinders mounted in an airstream. Ph.D. thesis, University of Cambridge 1962.
- [6] H. Connors. Fluidelastic vibration of tube arrays excited by cross flow. *Proc. ASME Winter Annual Meet., 1970* .
- [7] R. Blevins. Fluid elastic whirling of a tube row. *Journal of Pressure Vessel Technology* 96, (1974) 263–267.
- [8] C. Dalton and R. A. Helfinstine. Potential flow past a group of circular cylinders. *Journal of Fluids Engineering* 93, (1971) 636–642.
- [9] H. Tanaka and S. Takahara. Fluid elastic vibration of tube array in cross flow. *Journal of sound and vibration* 77, (1981) 19–37.
- [10] Y. Hassan, T. Bagwell, and D. Steininger. Large eddy simulation of the fluctuating forces on a square pitched tube array and comparison with experiment. *Flow-Induced Vibration, PVP* 189, (1990) 45–50.
- [11] J. Lever and D. Weaver. On the stability of heat exchanger tube bundles, part i: Modified theoretical model. *Journal of Sound and vibration* 107, (1986) 375–392.
- [12] W. Xia and L. Wang. The effect of axial extension on the fluidelastic vibration of an array of cylinders in cross-flow. *Nuclear Engineering and Design* 240, (2010) 1707–1713.
- [13] L. Wang, H. Dai, and Y. Han. Cross-flow-induced instability and nonlinear dynamics of cylinder arrays with consideration of initial axial load. *Nonlinear Dynamics* 67, (2012) 1043–1051.

- [14] L. Wang and Q. Ni. Hopf bifurcation and chaotic motions of a tubular cantilever subject to cross flow and loose support. *Nonlinear Dynamics* 59, (2010) 329–338.
- [15] A. Khalifa, D. Weaver, and S. Ziada. A single flexible tube in a rigid array as a model for fluidelastic instability in tube bundles. *Journal of Fluids and Structures* 34, (2012) 14–32.
- [16] S. Price and M. Paidoussis. An improved mathematical model for the stability of cylinder rows subject to cross-flow. *Journal of Sound and Vibration* 97, (1984) 615–640.
- [17] D. Weaver, S. Ziada, M. Au-Yang, S. Chen, M. Paidoussis, and M. Pettigrew. Flow-induced vibrations in power and process plant components progress and prospects. *Journal of Pressure Vessel Technology* 122, (2000) 339–348.
- [18] R. Azizian and N. Mureithi. A Simple Empirical Model for Tube–Support Normal Impact Interaction. *Journal of Pressure Vessel Technology* 136, (2014) 051,303.
- [19] A. Simpson and J. Flower. An improved mathematical model for the aerodynamic forces on tandem cylinders in motion with aeroelastic applications. *Journal of Sound and Vibration* 51, (1977) 183–217.